

RESEARCH ARTICLE

10.1002/2016JD024867

Geostationary satellite-based 6.7 μm band best water vapor information layer analysis over the Tibetan Plateau

Key Points:

- BWIL from Chinese GEO observations over the Tibetan Plateau and its seasonal and diurnal variation
- Topography and surface characteristics impact on the BWIL height and magnitude
- The difference on BWIL between over the Tibetan Plateau and over other regions in China

Correspondence to:

Y. Ai,
yufei.ai@ssec.wisc.edu

Citation:

Di, D., Y. Ai, J. Li, W. Shi, and N. Lu (2016), Geostationary satellite-based 6.7 μm band best water vapor information layer analysis over the Tibetan Plateau, *J. Geophys. Res. Atmos.*, 121, 4600–4613, doi:10.1002/2016JD024867.

Received 28 JUL 2015

Accepted 18 APR 2016

Accepted article online 23 APR 2016

Published online 7 MAY 2016

Di Di¹, Yufei Ai^{2,3}, Jun Li², Wenjing Shi^{2,4}, and Naimeng Lu⁵

¹Chinese Academy of Meteorological Sciences, China Meteorological Administration, Beijing, China, ²Cooperative Institute for Meteorological Satellite Study, University of Wisconsin-Madison, Madison, Wisconsin, USA, ³Laboratory for Climate and Ocean-Atmosphere Studies, Department of Atmospheric and Oceanic Sciences, School of Physics, Peking University, Beijing, China, ⁴State Key Laboratory of Numerical Modeling for Atmospheric Sciences and Geophysical Fluid Dynamics, Institute of Atmospheric Physics, Chinese Academy of Sciences, Beijing, China, ⁵National Satellite Meteorological Center, China Meteorological Administration, Beijing, China

Abstract The best water vapor information layer (BWIL) of the 6.7 μm water vapor absorption infrared (IR) band for the FengYun-2E is investigated over the Tibetan Plateau with standard atmospheric profile and European Centre for Medium-Range Weather Forecasts (ECMWF) operational model analysis data. The sensitivity tests show that surface characteristics over the Tibetan Plateau have a significant influence on the BWIL. To be specific, topographic elevation, colder skin temperature, and lower emissivity tend to lift the altitude of the BWIL, decrease its magnitude, and narrow the half-width range. The results from statistical analysis indicate that the altitude of the BWIL reaches the highest in summer and the lowest in winter. Meanwhile, the altitude of the BWIL is highly correlated with the water vapor amount above 500 hPa over the Tibetan Plateau and above 300 hPa over the East China Plain, respectively. The diurnal variation in the BWIL is synchronous with the diurnal variation in the surface skin temperature. It can be concluded from the study that surface characteristics over high terrain in dry and cold atmospheres have more significant impacts on the BWIL. With multiple water vapor absorption IR bands, the imagers on board the new generation of geostationary satellites will provide crucial improvement in water vapor remote sensing over the current single water vapor band on board the FY-2 series according to the analysis in this study.

1. Introduction

Water vapor comprises only 1–4% (by volume) of the atmosphere, yet it plays a critical role in the Earth's energy balance and severe weather forecasting. Water vapor absorbs and reradiates electromagnetic radiation in various wavelength bands, most notably the infrared 6.0–7.0 μm band. Such infrared (IR) radiation emitted by the Earth/atmosphere and measured by satellites is the basis for remote sensing tropospheric water vapor in the atmosphere.

The first geostationary Earth orbit (GEO) satellite with water vapor imaging capability was the European Meteosat-1 launched in 1977. The Meteosat series carry imaging radiometers with a 5.7–7.1 μm water vapor (WV) absorption band [Morel *et al.*, 1978]. The first Chinese geostationary satellite FengYun (FY)-2B (launched in 2000) includes a 6.3–7.6 μm WV band [Zhang *et al.*, 2006]. Current GEO satellites in operation all have at least one WV band centered between 6.0 and 7.5 μm .

The water vapor Jacobian function ($dT_b/d \ln q$) shows the sensitivity of the measured radiance to the change in water vapor concentration at a given pressure level p in the atmosphere. Therefore, it is able to reflect the remote sensing capability and limitation of the given channel [Bai *et al.*, 2014] and plays a significant role in moisture profile retrieval [Li, 1994; Li *et al.*, 2000] and radiance assimilation analysis [Chen *et al.*, 2010]. The atmospheric pressure layer corresponding to the minimum of the Jacobian function ($dT_b/d \ln q$) of the 6.7 μm band is also defined as the best water vapor information layer (BWIL) [Zeng, 1974]; it usually maxes out around 400 hPa, which means that the radiance is the most sensitive to the water vapor changes at this layer. As a result, water vapor in the middle-upper troposphere can be observed with this IR band. Water vapor is therefore a “passive tracer” which can be used to represent horizontal and vertical atmospheric motions on the mesoscale and synoptic scale [Petersen *et al.*, 1983, 1984; Narayanan *et al.*, 1989]. Due to the sensitivity of the 6.7 μm band to water vapor between 200 and 500 hPa, it is widely applied in tracking WV features over

the globe including cloud detection [Tokuno and Tsuchiya, 1994; Tian et al., 2004; Aumann et al., 2011], the retrieval of upper tropospheric relative humidity [Soden and Bretherton, 1993, 1994, 1996, Soden, 2000; Huang et al., 2004], deriving atmospheric motion winds [Tokuno, 1996; Velden, 1996; Velden et al., 1997], and analyzing the development of weather systems such as tornadoes, tropical cyclones, and deep convection [Allison et al., 1972; Manney and Stanford, 1987; Le Marshall, 1998; Bosart et al., 2000]. Combined with other bands, the 6.7 μm band can also help in estimating precipitation and longwave radiances from the Earth [Mishra, 2013; Park et al., 2015].

Fischer et al. [1981] demonstrated that for WV bands the contribution functions which reflect the sensitivity of emitted radiation by water vapor depend on the vertical water vapor profile and viewing angle; the sensitivity to temperature changes in the atmosphere is comparatively small, and the half-width center of the contribution functions lies between 560 and 360 hPa. The major contributing layer is about 320 hPa thick, and its location varies between 800 and 250 hPa. Poc et al. [1980] had similar results: the peak altitude of the contributions to the radiances varies from 550 hPa to 450 hPa over western Europe and the Mediterranean Sea. A relationship between the radiative response and the water vapor mass above the 600 hPa level is found in the same region. It should be noted that the contribution function has the same meaning of the Jacobian function in this study. However, previous studies focused on the water vapor observations over the sea surface or flat low land rather than over the plateaus. The impact of high terrain on the water vapor Jacobian function has not been studied thoroughly.

The Tibetan Plateau covers most of the Tibet Autonomous Region and Qinghai Province in western China, stretching approximately 1000 km north to south and 2500 km east to west, with an average elevation exceeding 4500 m. It is one of the most intense solar radiation regions in the world. Due to the thin air mass over the high terrain, the temperature and moisture changes over the Tibetan Plateau are approximately twice that over the low terrain given the same amount of heat and water vapor [Ye, 1981]. The weather and climate processes over China and adjacent regions have some unique features due to the Tibetan Plateau. The seasonal monsoon wind shift and weather associated with the heating and cooling of the Tibetan Plateau is the strongest on Earth. The upper air westerly jet streams are bifurcated into two branches due to the physical obstruction of the Himalayas and Tibetan Plateau. One branch is located to the south of the Himalayas, while the other is to the north of the Tibetan Plateau. The evolution of the two branches initiates the Indian monsoon circulation. The formation and evolution of the monsoon weather over China and other parts of Asia are influenced by the Tibetan Plateau [Flohn, 1968; Hahn and Manabe, 1975]. Due to the lack of conventional atmospheric water vapor observations over the Tibetan Plateau region, satellite-based measurements are crucial for understanding the water vapor distribution and transport associated with weather and climate systems such as monsoons over East Asia. Therefore, the study of BWIL over the Tibetan Plateau will help in the better utilization of WV IR bands to study the water vapor transport and variations over plateaus and to understand the thermal, dynamical, meteorological, and climatological influence of the Tibetan Plateau.

The motivations for studying the BWIL of the 6.7 μm band over the Tibetan Plateau are the following:

1. It is well known that the broadband centered at 6.7 μm is able to detect water vapor in the middle and upper troposphere. The detected information comes mainly from the layer centered around the BWIL. What are the distribution characteristics of the BWIL over the Tibetan Plateau region spatially, vertically, and temporally? The BWIL from this band and its variations over the plateaus might be significant and still not be quantified by other studies.
2. The impact of surface characteristics on Jacobian functions has already been studied theoretically [Zeng, 1974; Li, 1994; Li et al., 1994, 2000], but the demonstration and verification over the plateaus are still needed. The optical path is shortened from IR observations over high terrain regions due to a smaller amount of water vapor than in other regions with similar latitudes. Thus, the change in surface characteristics over the Tibetan Plateau might alter the Jacobian functions by some extent.
3. The new generation of GEO satellite imagers such as the Advanced Baseline Imager (ABI) [Schmit et al., 2005] have multiple water vapor absorption IR bands. China will have a similar imager called AGRI (Advanced Geostationary Radiation Imager) on board the FY-4 series, and the Tibetan Plateau region is well covered by FY-4. The new imager will provide improved vertical atmospheric moisture information over the current

imager with only a single water vapor IR band. Therefore, it is important to understand the improved capability for water vapor remote sensing over the Tibetan Plateau region from the new generation GEO imager over the current one.

This study analyzes the water vapor information features observed by FY-2E in 2014. The model, observation data, and calculation methodology are explained in section 2. Section 3 describes the impact of surface characteristics (topographic elevation, surface skin temperature, and surface IR emissivity) on the water vapor Jacobian function. Section 4 analyzes the seasonal and diurnal variations in the BWIL over the Tibetan Plateau and East China Plain. Section 5 shows the improvement with the next generation GEO satellite that carries three WV bands. The last section gives a summary and discussion.

2. Model and Data

The radiative transfer model (RTM) used in the study is the Pressure-Layer Fast Algorithm for Atmospheric Transmittance (PFAAST), developed by using line-by-line RTM calculations and the high-resolution transmission molecular absorption spectroscopic database HITRAN 2000 [Hannon *et al.*, 1996; Li *et al.*, 2004]. The model input includes 101-level atmospheric vertical profiles of temperature, water vapor concentration, and ozone, which are from the European Centre for Medium-Range Weather Forecasts (ECMWF) analysis data set in this study. The ECMWF analysis fields data are from the T799/L91 spectral model with a top at 0.01 hPa that became operational in February 2006 [Untch *et al.*, 2006; Manney *et al.*, 2008] and are available every 6 h (00, 06, 12, and 18 UTC) with a spatial resolution of 0.25°. The profiles are interpolated to the standard 101 atmospheric pressure levels before input to PFAAST. The surface properties, satellite zenith, and specific band information are also required for radiance and Jacobian function calculations. The surface IR emissivity is set by using the global IR land surface emissivity database [Seemann *et al.*, 2008] developed at the Cooperative Institute for Meteorological Satellite Studies (CIMSS) of the University of Wisconsin-Madison. The simulated band in this study is the WV band (centered at 6.7 μm) from FY-2E. Launched in 2008, the FY-2E satellite is at geostationary orbit with height of 35,800 km.

Our studies focus on the BWIL analysis of the WV band over the Tibetan Plateau. First, two regions are selected for the comparison of Jacobian functions over the Tibetan Plateau (30–35°N and 85–100°E) and the East China Plain (30–40°N and 115–120°E), respectively. The map in Figure 1 shows the locations of the two regions, as well as the elevation of China. Some surface characteristics affecting the Jacobian function have been selected by theoretical analysis—surface skin temperature, surface IR emissivity, and topographic elevation. Three sensitivity tests are then conducted with the standard atmospheric profile of middle-latitude winter as the model input data. In order to obtain practical and climatological conclusion, the Jacobian functions of the FY-2E WV band are calculated with each ECMWF analysis profile in January, April, July, and October 2014 by PFAAST. The seasonal and diurnal variations in the altitude and magnitude of BWIL are analyzed to investigate the remote sensing range of the WV band.

3. Impact of Surface Characteristics on BWIL

The approximation of the analytical water vapor Jacobian [Li, 1994; Li *et al.*, 2000] of a WV absorption band can be written as

$$W_q(p) = \left[(T_s - T_a)\epsilon\tau_s\beta_s - 2(1 - \epsilon) \int_0^{p_s} \beta\tau^* \frac{\partial T}{\partial p} dp \right] \frac{\partial \ln \tau_w}{\partial p} + \left\{ \int_p^{p_s} \beta[\tau + (1 - \epsilon)\tau^*] \frac{\partial T}{\partial p'} dp' \right\} \frac{\partial \ln \tau_w}{\partial p} \quad (1)$$

where $W_q(p)$ is the Jacobian function or water vapor mixing ratio weighting function of an atmospheric state at atmospheric pressure level p ; ϵ is the surface IR emissivity; p_s is surface pressure; T is the temperature of atmosphere at pressure level p ; T_s is surface skin temperature; T_a is surface air temperature; τ_w is water vapor component transmittance; τ is the total transmittance of the atmosphere above pressure level p ; τ_s is the surface transmittance; and $\tau^* = \tau_s^2/\tau$. $\beta(p) = [\partial B(p)/\partial T(p)]/(\partial R/\partial T_B)$, where B and T are the Planck radiance and atmospheric temperature, respectively, which are functions of pressure level p ; R is spectral radiance of a given IR band; and T_B is the corresponding brightness temperature. This analytical Jacobian calculation is accurate (e.g., comparable to the brute force numerical perturbation method) and computationally efficient. It has been used by the International ATOVS Processing Package (IAPP) [Li *et al.*, 2000], European Organisation for the Exploitation of Meteorological Satellites Nowcasting SAF processing package

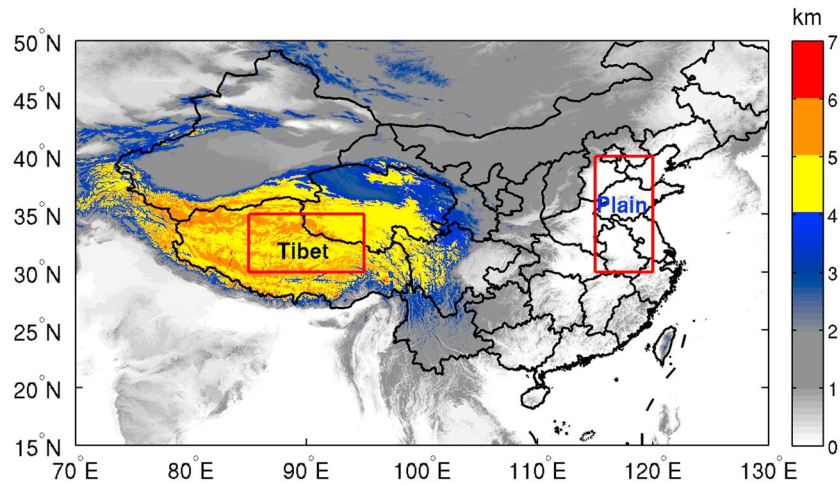


Figure 1. Elevation distribution over China and adjacent regions. Two red rectangles denote the regions selected to represent the Tibetan Plateau (Tibet) and the East China Plain (Plain), respectively.

(http://www.nwscf.org/scidocs/Documentation/SAF-NWC-CDOP2-INM-SCI-ATBD-13_v2.0.pdf), the operational GOES Sounder and GOES-R moisture product generation [Li et al., 2008; Jin et al., 2008], and Moderate Resolution Imaging Spectroradiometer (MODIS) atmospheric product generation in the International MODIS and Atmospheric Infrared Sounder Processing Package (IMAPP) (<http://cimss.ssec.wisc.edu/imapp/>) [Weisz et al., 2007], for operational and real-time applications.

In this study, three feature parameters related to BWIL are analyzed as illustrated in Figure 2b by using the standard atmospheric profile of middle-latitude winter as PFAAST input (the water vapor profile is shown in Figure 2a). Considering the high terrain of the Tibetan Plateau, the surface pressure is set as 600 hPa. The minimum value of $W_q(p)$ is regarded as the magnitude of the BWIL, denoted as M (a negative value because water vapor usually blocks the view of the satellite sensor—it should be pointed out that all the discussions of M only consider its numerical value in this paper, i.e., $|M|$); P is the height (measured by pressure layer) when $W_q(p)$ reaches M ; and dP is the full width at the half minimum of the Jacobian function peak, which is calculated as the difference between two pressure levels when $W_q(p)$ reaches half of the minimum

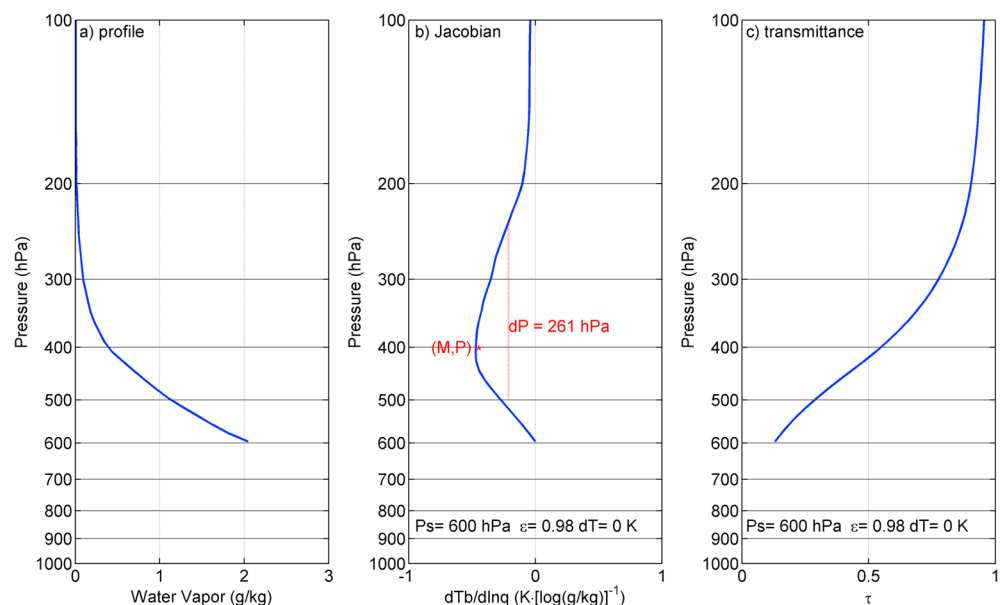


Figure 2. The atmospheric profile of middle-latitude winter above 600 hPa as input in PFAAST. (a) The input water vapor profile. (b) The calculated Jacobian function. (c) The atmospheric transmittance profile for the FY-2E WV IR band. The red dashed line in Figure 2b denotes the location of $M/2$.

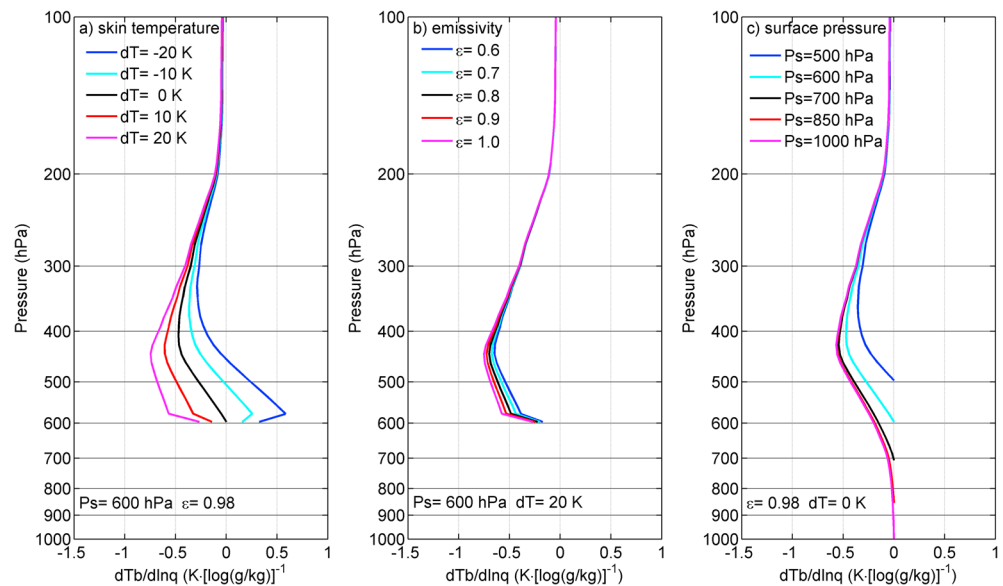


Figure 3. The sensitivity tests of surface characteristics for (a) surface skin temperature, (b) surface IR emissivity, and (c) surface pressure on the WV Jacobian over the Tibetan Plateau.

value ($M/2$). Theoretically, the radiative response represented by the Jacobian function shows the largest sensitivity (described as M) when the WV amount changes around layer P . dP shows the depth of the pressure layer which is sensitive to the change in WV amount. The physical meaning of the three parameters corresponding to BWIL can be summarized as below:

1. P reflects the height (pressure layer) of BWIL at which the IR radiance is the most sensitive to water vapor change, which means that this IR band can best sense the water vapor at this layer.
2. M reflects part of the water vapor information content contained in the IR radiance; for example, with similar BWILs, larger $|M|$ (numerical value) means better moisture sensitivity and remote sensing capability.
3. dP reflects the broad layer that the moisture information contained in IR band radiance mostly come from. Usually, it corresponds to the spectral coverage of this IR band; for example, a narrower spectral coverage in the IR region usually results in a smaller dP , which is why a geostationary hyperspectral IR sounder with high spatial, vertical, and temporal resolutions is required for atmospheric moisture profiling [Wang *et al.*, 2007; Schmit *et al.*, 2009].

3.1. Surface Skin Temperature

Theoretically, the surface properties shown as the first term in the equation (1) have a large influence on the magnitude of $W_q(p)$, and the influence on the Jacobian function will increase as the terrain elevates since the optical path in the second term will shorten. It is apparent that the increase in $dT = T_s - T_a$ tends to increase the magnitude of $W_q(p)$ when other variances remain unchanged in equation (1).

In the sensitivity tests of Figure 3a, dT is changed from -20 K to 20 K with an interval of 10 K when keeping ϵ as 0.98 and p_s as 600 hPa. The standard atmospheric middle-latitude winter profile is used in this calculation. Figure 3a simulates the effect of dT on the water vapor Jacobian functions over the Tibetan Plateau. The results indicate that a colder T_s compared with T_a tends to elevate the height of BWIL (smaller values of P) while also decreasing M and dP . However, the Jacobian functions in the upper atmosphere (over 400 hPa) are less affected. Another interesting fact is that when the surface skin temperature is cold enough (over 10 K colder than the atmosphere), water vapor near the surface tends to make a positive contribution to radiances according to the Jacobian functions shown in Figure 3a. It indicates that more water vapor information near the surface will be measured by the infrared WV band if $|dT|$ is large enough. Otherwise, if the surface air temperature and the surface skin temperature are very close, the water vapor information near the surface contributes little to the IR radiation with very small value of Jacobian function shown in Figure 3a. It suggests that the capability of IR remote sensing of near-surface water vapor is limited under this circumstance because satellite cannot distinguish the radiation emitted by the near-surface water vapor air mass and that by the Earth surface if $|dT|$ is close to 0 , which is consistent with the theoretic analysis by Zeng [1974] and Li [1994].

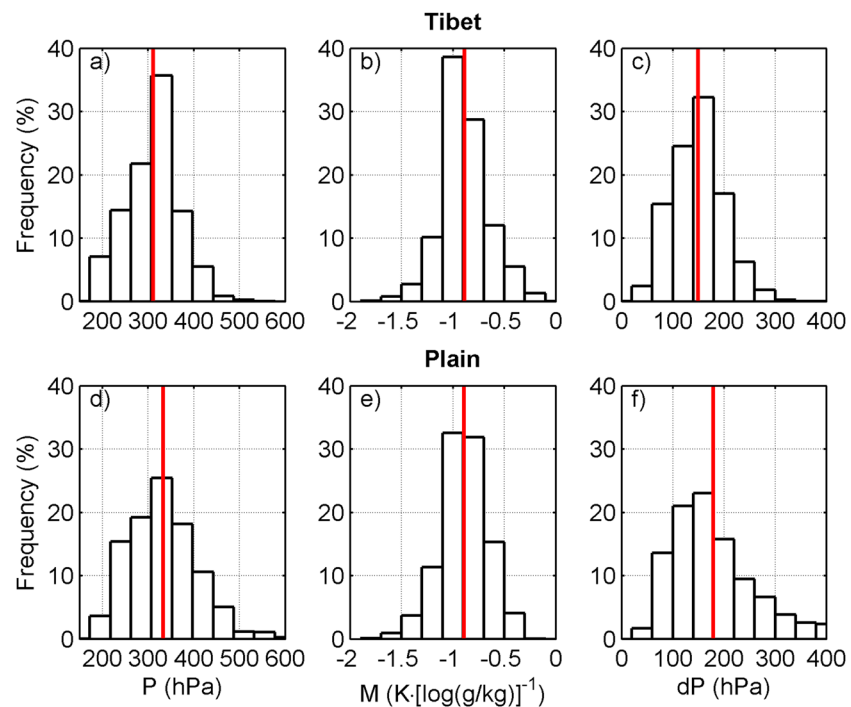


Figure 4. The frequency distribution of P , M , and dP (a–c) over the Tibetan Plateau and (d–f) over the East China Plain, respectively. Corresponding mean values are traced with red solid lines.

3.2. Surface IR Emissivity

Similarly, the variation in ϵ will have a certain impact on $W_q(p)$ if dT is not close to 0. When dT is positive, an increase in ϵ tends to increase the first term in equation (1), which means that an increase in ϵ will increase the magnitude of $W_q(p)$. On the other hand, if dT is negative, an increase of ϵ will decrease the magnitude of $W_q(p)$.

Figure 3b reveals the effect of surface IR emissivity on the WV Jacobian function where ϵ varies from 0.6 to 1.0 with an interval of 0.1 when dT is 20 K and p_s is 600 hPa. The results indicate that a smaller ϵ also tends to decrease M and dP when dT is positive, but not as significantly as the change caused by dT ; the Jacobian functions in the upper atmosphere (over 400 hPa) are little affected by surface IR emissivity. P also does not show a remarkable change when ϵ varies. The fact is that the surface IR emissivity for this region in January 2014 was about 0.95 to 0.99 according to Global Infrared Land Surface Emissivity data from the UW-Madison Baseline Fit Emissivity Database [Seemann *et al.*, 2008]. Therefore, in general surface IR emissivity (or epsilon) does not have a significant impact on BWIL over the Tibetan Plateau.

3.3. Topographic Elevations

The integration path of the second term in equation (1) is shorter over Tibet, which will theoretically give a smaller value for this term. In addition, the topographic elevation and dry upper and middle troposphere atmosphere result in a larger τ_s over the plateau, which will also generate a larger first term in equation (1). Therefore, it is not easy to predict the impact of topographic elevation on Jacobian functions in theory.

To show the impact of topographic elevation, the sensitivity tests are conducted in which p_s is set as 1000 hPa, 850 hPa, 700 hPa, 600 hPa, and 500 hPa when dT is 0 K and ϵ is 0.98. The results in Figure 3c actually indicate that topographic elevation tends to lift the height of BWIL while decreasing M and dP over the Tibetan Plateau, especially when the surface pressure is less than 700 hPa. The results suggest that the effect of the shorter integration path of the second term of equation (1) is more significant than that of the drier upper and middle troposphere environment, probably because the impact by the first term of equation (1) becomes smaller when $dT = 0$. Since the Jacobian values are close to zero near the surface, and the BWIL is in between surface and upper troposphere when $dT = 0$, the BWIL will be lifted upward if the surface altitude increases.

Based on the analysis above, since the altitude of the Tibetan Plateau is over 700 hPa, the Jacobian functions over the plateau are likely to have higher P and smaller dP values compared to those over the East China Plain.

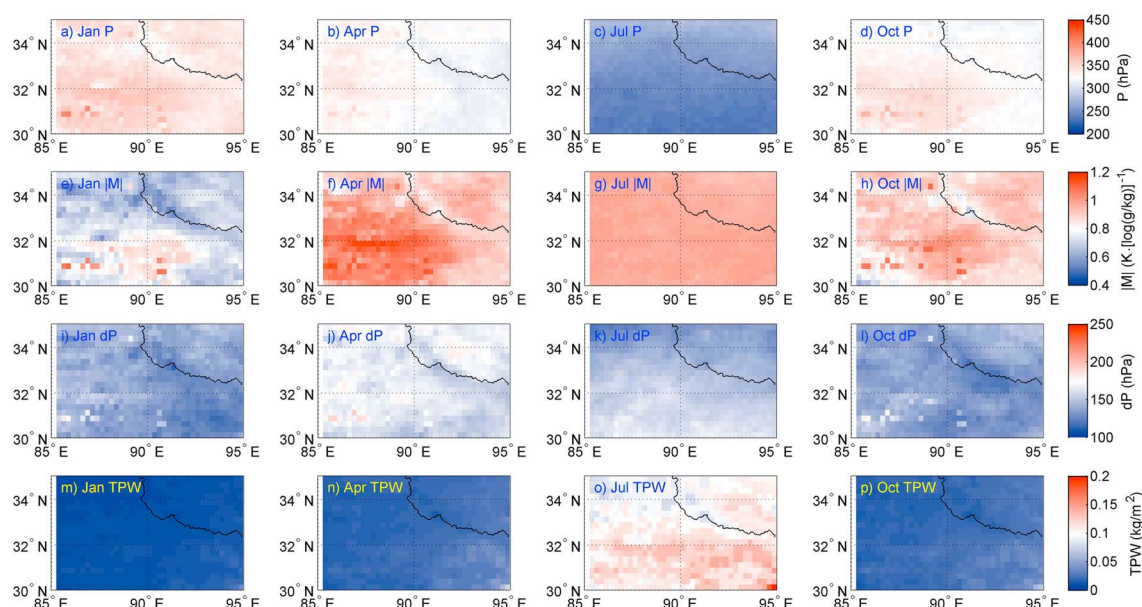


Figure 5. The mean P , M , and dP of BWIL and TPW over the Tibetan Plateau regions in (a, e, i, and m) January, (b, f, j, and n) April, (c, g, k, and o) July, and (d, h, l, and p) October.

Subsequent statistical analysis is conducted to confirm the conclusion obtained above by using the 91-level ECMWF operational model analysis data. The results of P , M , and dP are calculated at each grid over the Tibetan Plateau and East China Plain at 00, 06, 12, and 18 UTC. Statistically (shown in Figures 4a, 4c, 4d, and 4f), the variations in P and dP are larger over the East China Plain than over Tibet. The mean values of P (Figures 4a and 4d) and dP (Figures 4c and 4f) are also larger over the East China Plain than over the Tibetan Plateau by 22 hPa and 29 hPa, respectively, which demonstrates that topographic elevation lifts the height of BWIL and narrows dP . It can be seen in Figures 4b and 4e that M has a slightly larger variance over the Tibetan Plateau compared to over the East China Plain, while the mean value is almost the same for both regions. Additionally, it is found that lower P tends to have a larger M and a smaller dP over the East China Plain (not shown). But the correlations between these parameters are not significant over the Tibetan Plateau. Therefore, it can be inferred that the surface characteristics along with the atmospheric conditions have complex effects on the BWIL over the Tibetan Plateau.

4. Seasonal and Diurnal Characteristics of FY-2E BWIL

4.1. Seasonal Variation

Analyzing the climate characteristics of the water vapor information layer (WIL) improves understanding and application of the water vapor imagery from FY-2E. Therefore, the seasonal variations in the BWIL over the Tibet Plateau and the East China Plain are discussed in this section. The Jacobian functions of the WV band are calculated over each grid at 00, 06, 12, and 18 UTC during the study period over the Tibetan Plateau and over the East China Plain, respectively. The monthly mean results of P , M (the numerical value), and dP are shown in Figures 5 and 6. Comparing the two figures, it is obvious that both the spatial and temporal variations in P and dP over the East China Plain are much larger than that over the Tibetan Plateau, and the variations in M are larger over the Tibetan Plateau than over the East China Plain, which is consistent with the analysis mentioned above (section 3).

For both regions, the height of BWIL increases (with decreasing values of P) from winter to summer and decreases from summer to winter, which corresponds to the seasonal distribution of moisture due to monsoon. Over the East China Plain, M and dP also have obvious seasonal variations that M is larger in summer and smaller in winter while dP is larger in winter and smaller in summer. Over the Tibetan Plateau, M is also comparatively the smallest in winter while its variance is not regular in other seasons. Similarly, dP does not change remarkably over high terrain.

Additionally, in summer, the inhomogeneous horizontal distributions of P , M , and dP occur over the west of the Tibetan Plateau which may relate to its mountainous surface (shown in Figure 1). However, over the

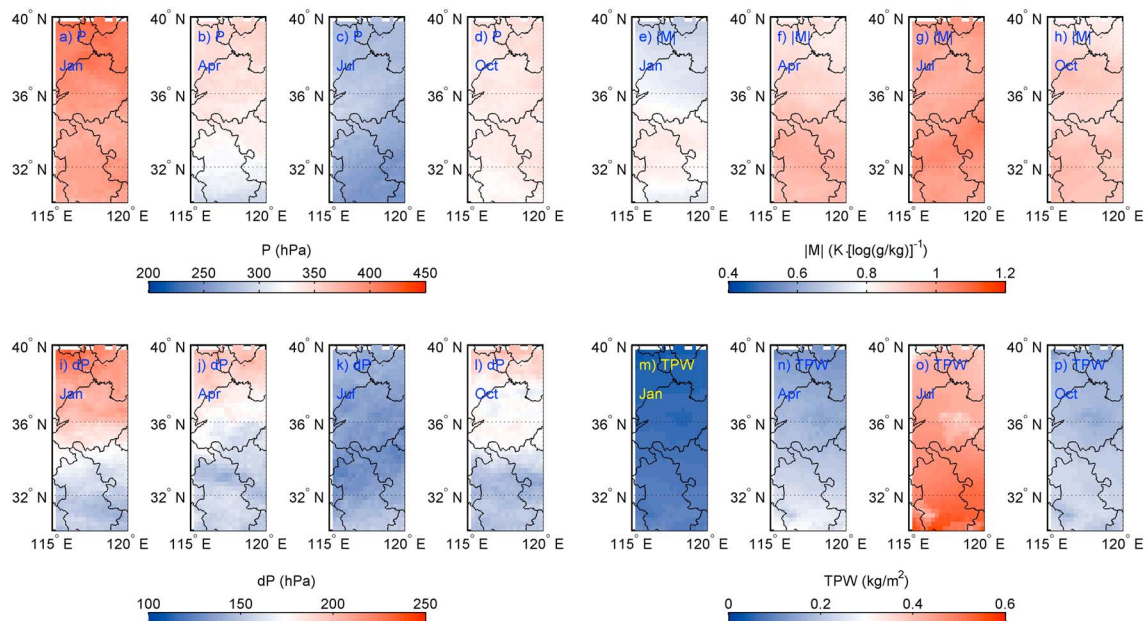


Figure 6. The mean P , M , and dP of BWIL and TPW over the East China Plain in (a, e, i, and m) January, (b, f, j, and n) April, (c, g, k, and o) July, and (d, h, l, and p) October.

East China Plain, the horizontal distributions of P , M , and dP show an obvious difference between the north and south of that region. The total precipitable water (TPW) seasonal variation shown in Figures 5 and 6 is dominated by regional monsoon which transports water vapor. The water vapor amount described by TPW reaches its peak in summer and its valley in winter for both the Tibetan Plateau and the East China Plain, which is the opposite phase as the variation of P and the same phase as the variation of M . In addition, the horizontal distributions of TPW also has inhomogeneous pattern consistent with that of P , M , and dP . Therefore, it indicates that the inhomogeneous horizontal distributions of these three parameters may be attributed to the water vapor transport during the monsoon.

To explicitly illustrate the role of moisture, the correlation coefficients between P and water vapor content (kg m^{-2}) within a certain atmospheric layer of 100–300 hPa, 300–500 hPa, 500–700 hPa, 700–850 hPa, 850 hPa to surface, and TPW are calculated for every profile over both regions. In Table 1, the negative values of the coefficients indicate that more water vapor content tends to result in a smaller P meaning higher height of BWIL, which is consistent with the theory. For the Tibetan Plateau, water vapor within 100–300 hPa and 300–500 hPa has more influence on P . For the East China Plain water vapor within 100–300 hPa and TPW has more influence. The correlation coefficients are larger over the Tibetan Plateau than over the East China Plain. Considering that there is less moisture over the Tibetan Plateau than over the East China Plain it can be inferred that the height of BWIL is more sensitive to the moisture change in the dry upper and middle troposphere.

4.2. Diurnal Variation

Based on the discussion above, it is clear that surface characteristics, especially the surface skin temperature, have a significant impact on the BWIL over the Tibetan Plateau. The diurnal variation in surface skin temperature is drastic over high terrain, which could affect the diurnal variation in BWIL over the Tibetan Plateau. To present the diurnal variation in the BWIL, the Jacobian functions are averaged from calculations every 6 h (00 UTC, 06 UTC, 12 UTC, and 18 UTC) over the Tibetan Plateau and the East China Plain for each month. It can be seen from Figure 7 that the diurnal variation in BWIL and dT are more significant over the Tibetan Plateau

Table 1. Correlation Coefficients Between P and Water Vapor Content (kg m^{-2}) of Different Atmospheric Layers

Atmospheric Layers	100–300 hPa	300–500 hPa	500–700 hPa	700–850 hPa	850 hPa to Surface	TPW
Tibet	–0.7015	–0.6661	–0.5777	–	–	–0.6570
Plain	–0.6223	–0.5643	–0.6017	–0.5949	–0.5594	–0.6323

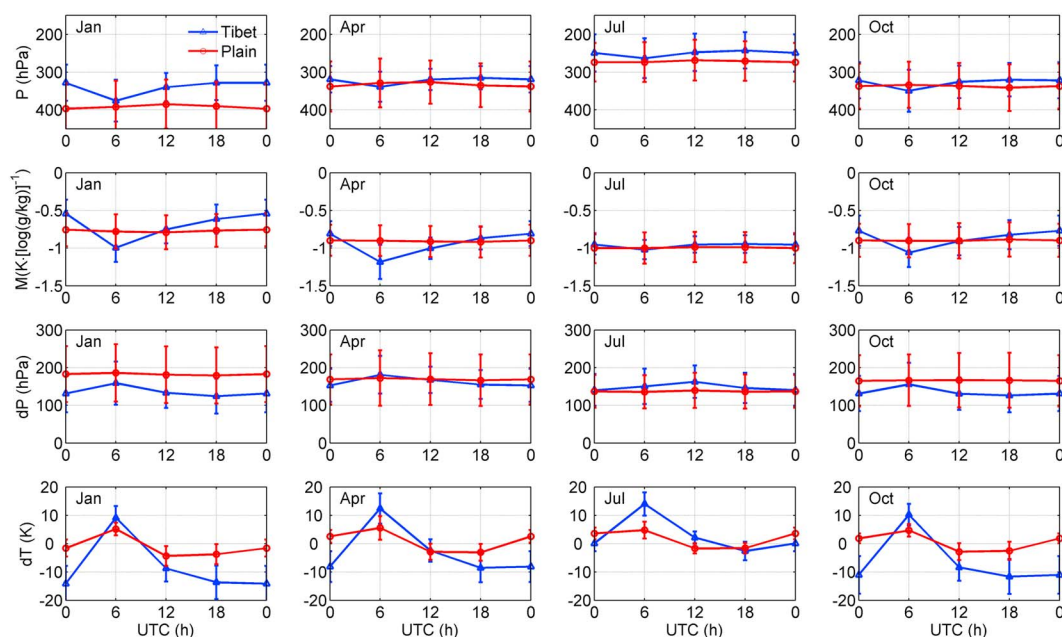


Figure 7. The diurnal variations for the mean of P , M , dP , and dT over the Tibetan Plateau and East China Plain in January, April, July, and October.

than over the East China Plain, especially in winter. Specifically, the diurnal variation of M and P is opposite to that of dT , while the diurnal variation in dP is the same over Tibet. The panels for January reveal that dT increases dramatically from morning (00 UTC) to noon (06 UTC) in winter when the atmosphere is cold and dry; this result might be partly attributed to the solar heating, which results in descended height of BWIL and increased $|M|$ and dP . However, the variation in dT does not have a significant effect on the BWIL over the Tibetan Plateau in July when moisture is the most abundant within the whole year. In addition to the fact that no significant diurnal variations are observed over the East China Plain where moisture is more abundant than the Tibetan Plateau, it can be inferred that in a dry and cold environment such as winter, the drastic diurnal variations in surface skin temperature have more significant impacts on the BWIL over high terrains such as the Tibetan Plateau.

5. Improvement With the Next Generation GEO Imager

The next generation GEO satellites (such as GOES-R, FY-4, MTG, and Himawari-8) are designed to be equipped with multiple water vapor absorption IR bands with peaks of Jacobian functions at different heights [Schmit et al., 2005; Stuhlmann et al., 2005; Zhang et al., 2006; Kurino, 2012]. The new generation of GEO imagers has similar water vapor vertical layer information compared to the current U.S. GOES Sounder and can be used together with numerical weather prediction (NWP) forecasts to continue the GOES Sounder legacy atmospheric products [Schmit et al., 2008]. Figure 8 shows the spectrum response functions (SRFs) of the WV bands of the Advanced Himawari Imager (AHI) on board the Japanese Himawari-8. The three bands of AHI are centered on different wavelengths, intending to detect water vapor information in multiple atmospheric layers.

The Jacobian functions of multiple AHI WV bands are simulated with results shown in Figure 9. In the test, the standard atmospheric profile of midlatitude winter is used as input to PFAAST for the FY-2E 6.7 μm band and AHI 6.21, 6.93, and 7.34 μm bands. In Figure 9, over both regions, the 6.21 μm band detects water vapor at a higher level around 380 hPa, the 6.93 μm band peaks at a similar level around 450 hPa as the 6.7 μm band of FY-2E, while the 7.34 μm band peaks at a lower level. Generally, the Jacobian functions over the Tibetan Plateau have higher BWIL and smaller M and dP as illustrated in Figure 9. Since the AHI 6.93 μm band and FY-2E WV band have the most spectral coverage overlap (see Figure 8), comparisons of P , M , and dP between the AHI 6.93 μm and the FY-2E 6.7 μm indicate that they have the similar M and P , but FY-2E has a much larger dP due to the much wider spectral coverage as analyzed (see the physical meaning of dP in section 3).

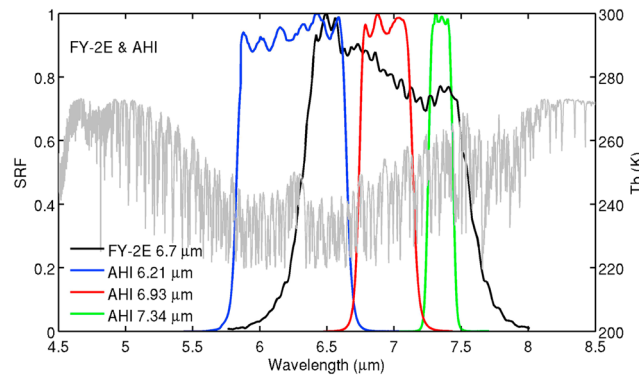


Figure 8. SRFs of water vapor absorption bands for FY-2E and Himawari-8/Advanced Himawari Imager (AHI). The gray line in the panel represents the high spectral resolution IASI (Infrared Atmospheric Sounding Interferometer) [Chalon et al., 2001] brightness temperatures of upwelling radiances at the TOA (top of the atmosphere) simulated with the standard atmospheric profile of middle-latitude winter.

It also shows that topographic elevation has a larger influence on the 6.7 μm band, 6.93 μm band, and 7.34 μm band which have the ability to detect moisture in the middle and lower atmospheric layers. The seasonal and diurnal variations for the three WV IR bands on AHI are similar to FY-2E (not shown).

As mentioned, the magnitude and BWIL of Jacobian function reflect the water vapor information content contained in the measured IR radiance, which determines the retrieval accuracy based on the information analysis. Thus, it can be inferred that the largest background (e.g., NWP forecast) error reduction or the best retrieval accuracy occurs around the BWIL theoretically. This part analyzes

the retrieval errors for both FY-2E and AHI to demonstrate the improvement from the next generation GEO imager over the current one. Besides, since the surface characteristics have impacts on the Jacobian function over the Tibetan Plateau, the analysis can also show their effects on the retrieval accuracy or the background error reduction. Most satellite retrieval methodologies based on optimal estimation theory assume that the error covariances of the observational and background information are known. For further error analysis, the background error covariance matrix (B) is calculated by using the National Meteorological Center (NMC) method and daily specific humidity forecasts from the Global/Regional Assimilation and Prediction System (GRAPES) model in December 2012. The NMC method can provide a climatological estimate of B with an assumption that B is well approximated by the averaged forecast difference statistics [Lee and Lee, 2011]:

$$B = \overline{(x_f - x_t)(x_f - x_t)^T} \approx \overline{(x_{24} - x_{12})(x_{24} - x_{12})^T} \quad (2)$$

where x_f and x_t denote forecast and true atmosphere state, respectively, and x_{24} and x_{12} represent 24 h and 12 h forecasts, respectively. In this study, B is obtained by calculating the difference between 24 h and 12 h forecasts twice a day for a whole month and the results of B over both regions are shown in Figures 10a and 10d.

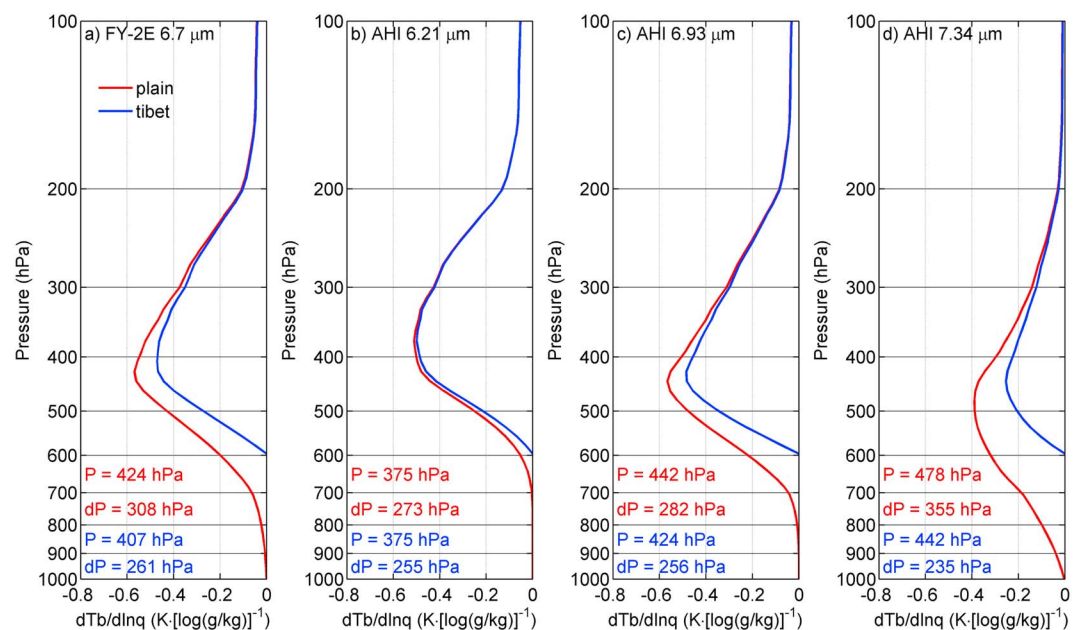


Figure 9. The Jacobian functions for WV bands on (a) FY-2E and (b–d) Himawari-8/AHI over the Tibetan Plateau and the East China Plain calculated by PFAAST using the standard atmospheric profile of middle-latitude winter.

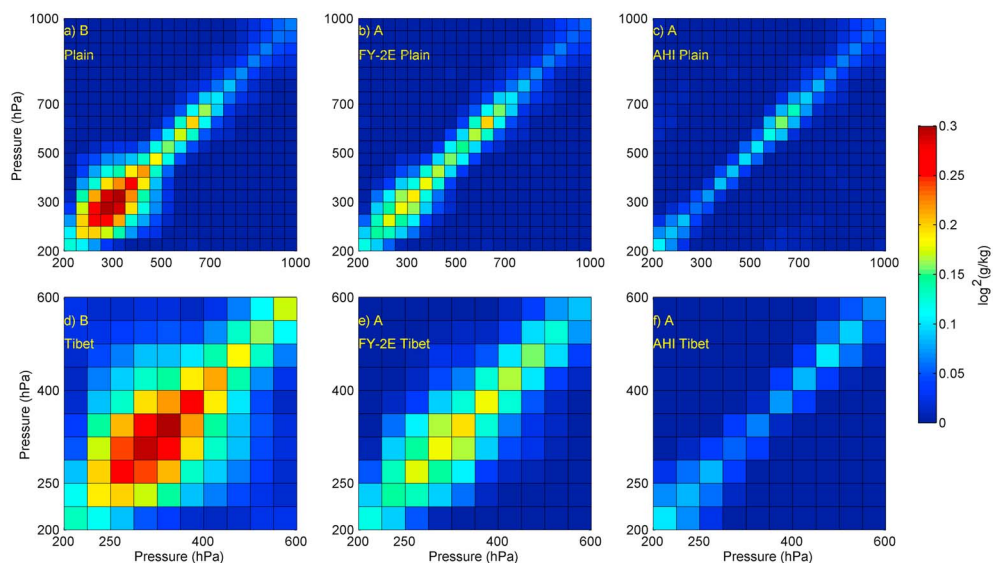


Figure 10. (a and d) The background error covariance matrix over the East China Plain and the Tibetan Plateau, respectively; (b and e) the analysis error covariance matrix over the East China Plain and the Tibetan Plateau for FY-2E; and (c and f) the analysis error covariance matrix over the East China Plain and the Tibetan Plateau for AHI.

The corresponding root-mean-square (RMS) error (Error B), which is the square root of the diagonal elements of B , over the East China Plain and the Tibetan Plateau region is represented in Figures 11a and 11b, respectively. The observation error matrix (E) of two sensors is estimated with the corresponding instrument precision index – noise equivalent temperature difference ($NE\Delta T$) and calculated brightness temperature. The analysis retrieval error matrix (A) can be determined by $A = (B^{-1} + K^T E^{-1} K)^{-1}$ if we ignore the retrieval error caused by the imperfect linearized radiance transfer equation and inverse model [Huang *et al.*, 1992]. In the equation, the matrix K is the Jacobian functions calculated by PFAAST model and ECMWF analysis data set, which for FY-2E is the Jacobian vector due to its single WV band while for AHI is the Jacobian matrix of multiple channels. The calculations of A for different sensor and regions are shown in Figure 10. The corresponding RMS error (Error A), which is the square root of the diagonal elements of A , over the East China Plain

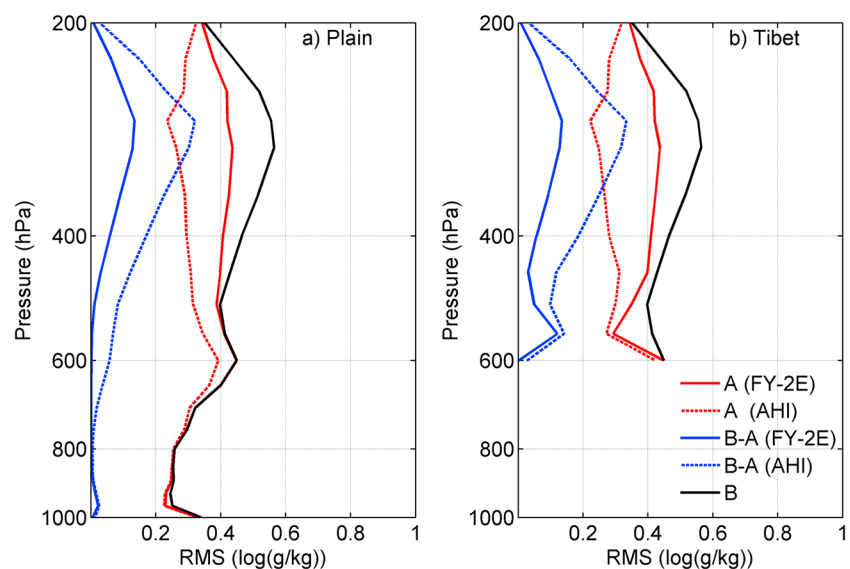


Figure 11. RMS background error (Error B, black solid line), RMS water vapor analysis retrieval error (Error A), and the difference between background error and analysis retrieval error (Error B – A) of FY-2E and AHI over the (a) Plain and (b) Tibet, respectively. The Error A of FY-2E and AHI is plotted as red solid and dashed lines, respectively. The Error B – A of FY-2E and AHI is shown as blue solid and dashed lines, respectively.

and the Tibetan Plateau region is represented in Figures 11a and 11b, respectively. In order to illustrate the role of the satellite sensor in retrieval error improvement, the difference between Error B and Error A of both areas and sensors is also shown in Figures 11a and 11b, respectively.

In general, a larger retrieval error improvement (Error B – A) appears in the upper and middle troposphere where the minimum of the WV Jacobian function can mostly be found. It indicates that extensive WV information detected by the two instruments is able to improve the retrieval performance. In Figures 11a and 11b, both over the Plain and Tibet, using AHI provides significant improvement in retrieval accuracy over using FY-2E, especially in the upper and middle troposphere. This result shows the superiority of the three WV bands on board AHI. In addition, a significant error improvement occurs in the near-surface layer over Tibet, which also indicates that the surface features affect the WV Jacobian functions near the surface over the plateau.

6. Summary and Future Work

This work studies the BWIL of the WV band for FY-2E over the Tibetan Plateau. In order to make comparisons, two representative regions are selected to be analyzed with different terrain heights. In this study, ECMWF operational model analysis data from 2014 and the standard atmospheric profile of middle-latitude winter are used for calculating the Jacobian functions of water vapor. The surface emissivity is taken from the global IR land surface emissivity database. The characteristics of BWIL are defined as the altitude P , the magnitude M , and half-width range dP . In this work, it is found that

1. Colder skin temperature (compared with the atmospheric temperature near the surface), smaller surface IR emissivity, and higher terrain tend to lift the height of BWIL (decrease P) and decrease M and dP . However, surface skin temperature and surface IR emissivity are only able to affect the Jacobian function below 400 hPa.
2. The height of BWIL increases from winter to summer and decreases from summer to winter for both regions, which corresponds to the seasonal distribution of moisture due to the monsoon. The seasonal variation patterns of M and dP are similar over the Plain, while the results over Tibet are more complicated. The inhomogeneous horizontal distributions of M and dP are attributed to the complex topography over the Tibetan Plateau. Water vapor within 100–300 hPa and 300–500 hPa has more influence on P over the Tibetan Plateau, while water vapor within 100–300 hPa and TPW has more influence over the Plain.
3. Based on analyzing the diurnal variations of BWIL, it is concluded that in a dry and cold environment such as winter, the drastic diurnal variations in surface skin temperature have more significant impacts on the water vapor Jacobian function over high terrain such as the Tibetan Plateau.

In addition, multiple WV IR bands are designed for the next generation GEOs such as Himawari-8 and FY-4, intending to detect WV information on multiple atmospheric levels. Our study shows that topographic elevation tends to decrease M , narrow dP , and lift the height of BWIL for the WV band which detects water vapor in the middle and low troposphere including the 6.7, 6.93, and 7.34 μm bands. Besides, we prove that AHI has greater retrieval accuracy than FY-2E over both the Plain and Tibet, especially in the upper and middle troposphere, according to the error analysis. Although AHI has been in orbit for more than 1 year, and the coverage over the Tibetan Plateau is near the viewing edge, more studies on the BWIL and its application on multi-layer moisture detection over the Tibetan Plateau will be conducted after the launch of the next generation of FengYun geostationary satellite (FY-4).

Acknowledgments

This research is supported by GYHY201306017 and GYHY201406011. The work is also partially funded by the China Scholarship Council (CSC) (201406010014). ECMWF is thanked for the operational model analysis data set. The surface IR emissivity data are from the UW-Madison Baseline Fit Emissivity (available at ftp://ftp.ssec.wisc.edu/pub/g_emis/). The PFAAST model was run on computers provided by the China Meteorological Administration (CMA) National Satellite Meteorological Center and UW-Madison Space Science Engineering Center (SSEC).

References

- Allison, L. J., J. Steranka, G. Thomas Cherrix, and E. Hilsenrath (1972), Meteorological applications of the Nimbus 4 Temperature-Humidity Infrared Radiometer, 6.7 micron channel data, *Bull. Am. Meteorol. Soc.*, *53*(6), 526–535.
- Aumann, H., S. DeSouza-Machado, and A. Behrangi (2011), Deep convective clouds at the tropopause, *Atmos. Chem. Phys.*, *11*(3), 1167–1176.
- Bai, W., C. Wu, J. Li, and W. Wang (2014), Impact of terrain altitude and cloud height on ozone remote sensing from satellite, *J. Atmos. Oceanic Technol.*, *31*(4), 903–912.
- Bosart, L. F., W. E. Bracken, J. Molinari, C. S. Velden, and P. G. Black (2000), Environmental influences on the rapid intensification of Hurricane Opal (1995) over the Gulf of Mexico, *Mon. Weather Rev.*, *128*(2), 322–352.
- Chalon, G., F. Cayla, and D. Diebel (2001), IASI: An advanced sounder for operational meteorology, *paper presented at 52nd Congress of IAF*, Toulouse, France, 1–5 Oct.
- Chen, Y., Y. Han, P. Van Delst, and F. Weng (2010), On water vapor Jacobian in fast radiative transfer model, *J. Geophys. Res.*, *115*, D12303, doi:10.1029/2009JD013379.
- Fischer, H., N. Eigenwillig, and H. Müller (1981), Information content of MeteoSat and Nimbus/THIR water vapor channel data: Altitude association of observed phenomena, *J. Appl. Meteorol.*, *20*(11), 1344–1352.

- Flohn, H. (1968), *Contributions to a Meteorology of the Tibetan Highlands*, Issue 130, Department of Atmospheric Science, Col. State Univ. Fort Collins, Colorado.
- Hahn, D. G., and S. Manabe (1975), The role of mountains in the South Asian monsoon circulation, *J. Atmos. Sci.*, 32(8), 1515–1541.
- Hannon, S. E., L. L. Strow, and W. W. McMillan (1996), Atmospheric infrared fast transmittance models: A comparison of two approaches, in *SPIE's 1996 International Symposium on Optical Science, Engineering, and Instrumentation*, pp. 94–105, International Society for Optics and Photonics, Denver, Colo.
- Huang, H.-L., W. L. Smith, and H. M. Woolf (1992), Vertical resolution and accuracy of atmospheric infrared sounding spectrometers, *J. Appl. Meteorol.*, 31(3), 265–274.
- Huang, Y., M. Wang, and J. Mao (2004), Retrieval of upper tropospheric relative humidity by the GMS-5 water vapor channel: A study of the technique, *Adv. Atmos. Sci.*, 21(1), 53–60.
- Jin, X., J. Li, T. J. Schmit, J. Li, M. D. Goldberg, and J. J. Gurka (2008), Retrieving clear-sky atmospheric parameters from SEVIRI and ABI infrared radiances, *J. Geophys. Res.*, 113, D15310, doi:10.1029/2008JD010040.
- Kurino, T. (2012), Future plan and recent activities for the Japanese follow-on geostationary meteorological satellite Himawari-8/9, *Abstract IN43E-03 presented at 2012 Fall Meeting, AGU, San Francisco, Calif.*, 3–7 Dec.
- Le Marshall, J. (1998), Cloud and water vapour motion vectors in tropical cyclone track forecasting: A review, *Meteorol. Atmos. Phys.*, 65(3–4), 141–151.
- Lee, S.-W., and D.-K. Lee (2011), Improvement in background error covariances using ensemble forecasts for assimilation of high-resolution satellite data, *Adv. Atmos. Sci.*, 28(4), 758–774.
- Li, J. (1994), Temperature and water vapor weighting functions from radiative transfer equation with surface emissivity and solar reflectivity, *Adv. Atmos. Sci.*, 11(4), 421–426.
- Li, J., F. Zhou, and Q. Zeng (1994), Simultaneous non-linear retrieval of atmospheric temperature and absorbing constituent profiles from satellite infrared sounder radiances, *Adv. Atmos. Sci.*, 11(2), 128–138.
- Li, J., W. W. Wolf, W. P. Menzel, W. Zhang, H.-L. Huang, and T. H. Achtor (2000), Global soundings of the atmosphere from ATOVS measurements: The algorithm and validation, *J. Appl. Meteorol.*, 39(8), 1248–1268.
- Li, J., J. P. Nelson III, C. C. Schmidt, T. J. Schmit, W. P. Menzel, S. Seemann, and B. Eva (2004), An approach to improvement temperature and moisture retrievals from the GOES sounder measurements, *paper presented at 13th Conference on Satellite Meteorology and Oceanography*, Am. Meteorol. Soc., Norfolk, Va., 20–23 Sep.
- Li, Z., J. Li, W. P. Menzel, T. J. Schmit, J. P. Nelson, J. Daniels, and S. A. Ackerman (2008), GOES sounding improvement and applications to severe storm nowcasting, *Geophys. Res. Lett.*, 35, L03806, doi:10.1029/2007GL032797.
- Manney, G. L., and J. L. Stanford (1987), On the relation of 6.7 μm water vapour features to isentropic distributions of potential vorticity, *Q. J. R. Meteorol. Soc.*, 113(477), 1048–1057.
- Manney, G. L., et al. (2008), The evolution of the stratopause during the 2006 major warming: Satellite data and assimilated meteorological analyses, *J. Geophys. Res.*, 113, D11115, doi:10.1029/2007JD009097.
- Mishra, A. K. (2013), A new technique to estimate precipitation at fine scale using multifrequency satellite observations over Indian land and oceanic regions, *IEEE Trans. Geosci. Remote Sens.*, 51(7), 4349–4358.
- Morel, P., M. Desbois, and G. Szejwach (1978), A new insight into the troposphere with water vapor channel of MeteoSat, *Bull. Am. Meteorol. Soc.*, 59, 711–714.
- Narayanan, M., P. Pal, P. Joshi, M. Mali, and B. Simon (1989), Observations of mid-tropospheric circulation from water vapour radiances of polar orbiting satellites, in *Proceedings of the Indian Academy of Sciences-Earth and Planetary Sciences*, vol. 98, pp. 247–254, Springer, India.
- Park, M.-S., C.-H. Ho, H. Cho, and Y.-S. Choi (2015), Retrieval of outgoing longwave radiation from COMS narrowband infrared imagery, *Adv. Atmos. Sci.*, 32(3), 375–388.
- Petersen, R. A., L. W. Uccellini, D. Chesters, A. Mostek, and D. Keyser (1983), The use of VAS satellite data in weather analysis, prediction, and diagnosis, *Nat. Weather Dig.*, 8, 12–23.
- Petersen, R. A., L. W. Uccellini, A. Mostek, and D. A. Keyser (1984), Delineating mid-and low-level water vapor patterns in pre-convective environments using VAS moisture channels, *Mon. Weather Rev.*, 112(11), 2178–2198.
- Poc, M., M. Roulleau, N. Scott, and A. Chedin (1980), Quantitative studies of MeteoSat water-vapor channel data, *J. Appl. Meteorol.*, 19(7), 868–876.
- Schmit, T. J., M. M. Gunshor, W. P. Menzel, J. J. Gurka, J. Li, and A. S. Bachmeier (2005), Introducing the next-generation Advanced Baseline Imager on GOES-R, *Bull. Am. Meteorol. Soc.*, 86(8), 1079–1096.
- Schmit, T. J., J. Li, W. F. Feltz, J. J. Gurka, M. D. Goldberg, and K. J. Schrab (2008), The GOES-R Advanced Baseline Imager and the continuation of current sounder products, *J. Appl. Meteorol. Climatol.*, 47(10), 2696–2711.
- Schmit, T. J., J. Li, S. A. Ackerman, and J. J. Gurka (2009), High-spectral-and high-temporal-resolution infrared measurements from geostationary orbit, *J. Atmos. Oceanic Technol.*, 26(11), 2273–2292.
- Seemann, S. W., E. E. Borbas, R. O. Knuteson, G. R. Stephenson, and H.-L. Huang (2008), Development of a global infrared land surface emissivity database for application to clear sky sounding retrievals from multispectral satellite radiance measurements, *J. Appl. Meteorol. Climatol.*, 47(1), 108–123.
- Soden, B. J. (2000), Diurnal cycle of convection, clouds, and water vapor in the tropical upper troposphere, *Geophys. Res. Lett.*, 27(15), 2173–2176.
- Soden, B. J., and F. P. Bretherton (1993), Upper tropospheric relative humidity from the GOES 6.7 μm channel: Method and climatology for July 1987, *J. Geophys. Res.*, 98(D9), 16,669–16,688.
- Soden, B. J., and F. P. Bretherton (1994), Evaluation of water vapor distribution in general circulation models using satellite observations, *J. Geophys. Res.*, 99(D1), 1187–1210.
- Soden, B. J., and F. P. Bretherton (1996), Interpretation of TOVS water vapor radiances in terms of layer-average relative humidities: Method and climatology for the upper, middle, and lower troposphere, *J. Geophys. Res.*, 101(D5), 9333–9343.
- Stuhlmann, R., et al. (2005), Plans for EUMETSAT's Third Generation MeteoSat geostationary satellite programme, *Adv. Space Res.*, 36(5), 975–981.
- Tian, B., B. J. Soden, and X. Wu (2004), Diurnal cycle of convection, clouds, and water vapor in the tropical upper troposphere: Satellites versus a general circulation model, *J. Geophys. Res.*, 109, D10101, doi:10.1029/2003JD004117.
- Tokuno, M. (1996), Operational system for extracting cloud motion and water vapor motion winds from GMS-5 image data, in *Proceedings of the Third International Winds Workshop*, pp. 21–30, EUMETSAT, Ascona, Switz.
- Tokuno, M., and K. Tsuchiya (1994), Classification of cloud types based on data of multiple satellite sensors, *Adv. Space Res.*, 14(3), 199–206.

- Untch, A., M. Miller, M. Hortal, R. Buizza, and P. Janssen (2006), Towards a global meso-scale model: The high-resolution system T799L91 and T399L62 EPS, *ECMWF Newsl.*, 108, 6–13.
- Velden, C. (1996), Positive impact of satellite-derived winds during the 1995 hurricane season: Example of optimizing data application and processing strategy, in *Proceedings of the Third International Winds Workshop*, pp. 81–89, EUMETSAT, Ascona Switz.
- Velden, C. S., C. M. Hayden, S. J. Nieman, W. P. Menzel, S. Wanzong, and J. S. Goerss (1997), Upper-tropospheric winds derived from geostationary satellite water vapor observations, *Bull. Am. Meteorol. Soc.*, 78(2), 173–195.
- Wang, F., J. Li, T. J. Schmit, and S. A. Ackerman (2007), Trade-off studies of a hyperspectral infrared sounder on a geostationary satellite, *Appl. Opt.*, 46(2), 200–209.
- Weisz, E., H.-L. Huang, J. Li, E. Borbas, K. Baggett, P. Thapliyal, and L. Guan (2007), International MODIS and AIRS processing package: AIRS products and applications, *J. Appl. Remote Sens.*, 1(1), 13519.
- Ye, D. (1981), Some characteristics of the summer circulation over the Qinghai-Xizang (Tibet) Plateau and its neighborhood, *Bull. Am. Meteorol. Soc.*, 62(1), 14–19.
- Zeng, Q. (1974), *Principle of Atmospheric Infrared Remote Sensing*, Science Press, Beijing.
- Zhang, W., M. J. Xu, M. C. Dong, and M. J. Yang (2006), China's current and future meteorological satellite systems, in *Earth Science Satellite Remote Sensing*, pp. 392–413, Springer, Berlin.